The Astronomical Journal, 124:2516–2523, 2002 November

RADIO-INFRARED SUPERNEBULAE IN II Zw 40

Sara C. Beck,[1] Jean L. Turner,[2] Laura E. Langland-Shula,[3] David S. Meier,[2,4]
Lucian P. Crosthwaite,[2,5] and Varoujan Gorjian[6]
Received 2002 May 27; accepted 2002 July 18

ABSTRACT

We report subarcsecond-resolution Very Large Array and Keck mid-infrared imaging of the dwarf starburst galaxy II Zw 40. II Zw 40 contains a bright compact thermal radio and infrared source with all the characteristics of a collection of dense H II regions ionized by at least 14,000 O stars. The supernebula is revealed to consist of multiple sources within an envelope of weaker emission. The radio emission is dominated by free-free emission at 2 cm, and the spectrum of this emission appears to be rising. This suggests that the free-free emission is optically thick at 2 cm and that the individual H II regions are ~1 pc in size. This complex of "supernebulae" dominates the total infrared luminosity of II Zw 40, although the radio source is less than ~150 pc in diameter. Multiple super–star clusters appear to be forming here, the much larger analogs of large Galactic H II region complexes.

Key words: galaxies: dwarf — galaxies: individual (II Zw 40) — galaxies: starburst — galaxies: star clusters — radio continuum

1. INTRODUCTION: INFRARED AND RADIO SUPERNEBULAE IN STARBURSTS

Starburst galaxies are distinguished by the concentration, not simply the quantity, of star formation. Optical and UV studies with the resolution of the *Hubble Space Telescope* (*HST*) have found star formation regions to contain super–star clusters, as populous and as dense as globular clusters but with ages of only a few million years. Observations in the radio and infrared are finding the even younger and obscured counterparts of these star clusters. Traced by optically thick free-free emission at centimeter wavelengths, radio-infrared "supernebulae" (Turner, Ho, & Beck 1998; Turner, Beck, & Ho 2000; Gorjian, Turner, & Beck 2001) or "ultradense H II regions" (Kobulnicky & Johnson 1999) have been discovered in nearby starburst galaxies. The discovery of these regions has been due to the development of subarcsecond imaging in the infrared and radio. These H II regions are bright and compact, excited by immense clusters of hot young stars, or "star-forming clumps" (Beck, Turner, & Gorjian 2001). The sources have in common all the signs of young star formation: high gas density (often greater than 10^4 cm^{-3}; Turner et al. 1998; Kobulnicky & Johnson 1999; Tarchi et al. 2000; Meier, Turner, & Beck 2002), a centimeter-wave continuum with spectral index from -0.1 to $+1.5$, substantial extinctions ($A_V > \sim 10$ mag; Kawara, Nishida, & Phillips 1989; Ho, Beck, & Turner 1990), and very strong mid-infrared emission (Gorjian et al. 2001; Beck et al. 2001; Dale et al. 2001; Vacca, Johnson, & Conti 2002). It is not just that these supernebulae are very luminous in the infrared; they may actually dominate the infrared emission of the entire galaxy. In the nearby dwarf galaxy NGC 5253, for example, at least 75% of the mid-infrared emission seen by *IRAS* and 25% of the total bolometric luminosity appear to come from one obscured star cluster less than 2 pc in diameter (Gorjian et al. 2001). In another starbursting dwarf, He 2-10, essentially all the mid-infrared emission is from star-forming clumps in a 200 pc by 50 pc disk (Beck et al. 2001; Vacca et al. 2002). If infrared emission traces and quantifies star formation, as has been thought since *IRAS*, then since these clusters or supernebulae are *the* sources of infrared; they are also *the* starburst.

II Zw 40 is a starburst dwarf galaxy 10.5 ($H_0/75$) Mpc away. It appears to be the result of a collision of two smaller galaxies (Baldwin, Spinrad, & Terlvich 1982; Brinks & Klein 1988; van Zee, Skillman, & Salzer 1998). At optical wavelengths it is dominated by one bright star cluster (Sargent 1970), which is also a strong source of Hα (Sargent & Searle 1970) and associated nebular lines (Walsh & Roy 1993), has the Wolf-Rayet feature (Vacca & Conti 1992), and in general has all the signs of a young star formation region. The infrared spectrum is dominated by high-excitation lines such as [Ne III] and [S IV] (Roche et al. 1991; Thornley et al. 2000; Beck, Crowther, & Conti 2002). The radio continuum emission is nearly all thermal emission (Klein, Weiland, & Brinks 1991; Klein, Wielebinski, & Thuan 1984; Jaffe, Perola, & Tarenghi 1978; Deeg et al. 1993), and the emission is relatively compact (Wynn-Williams & Becklin 1986; Sramek & Weedman 1986; Klein et al. 1991). Like the radio continuum, the Hα (Sargent & Searle 1970) and Brγ lines (Wynn-Williams & Becklin 1986; Moorwood & Oliva 1988; Joy & Lester 1988; Vanzi et al. 1996; Davies, Sugai, & Ward 1998) are bright in this galaxy. Molecular gas is conspicuous by its absence; Sage et al. (1992) remark on its unusually high star formation efficiency. In these respects, II Zw 40 resembles NGC 5253 (Crowther et al. 1999; Turner et al. 1998; Turner et al. 2000), probably the youngest, most massive, and most extreme example of an obscured young super–star cluster or supernebula in the local universe.

[1] Department of Physics and Astronomy, Tel Aviv University, 69978 Ramat Aviv, Israel; sara@wise1.tau.ac.il.
[2] Department of Physics and Astronomy, Box 951547, UCLA, Los Angeles, CA 90095; turner@astro.ucla.edu.
[3] Department of Astronomy and Astrophysics, 477 Clark Kerr Hall, University of California, Santa Cruz, CA 95064; laura@ucolick.org.
[4] Current address: Department of Astronomy, 1002 West Green Street, University of Illinois, Urbana, IL 61801; meierd@astro.uiuc.edu.
[5] Astute Networks, 16868 Via Del Campo Court, Suite 200, San Diego CA 92127; pat@astutenetworks.com.
[6] Jet Propulsion Laboratory, California Institute of Technology, MS 169-327, Pasadena, CA 91109; vg@jpl.nasa.gov.

Motivated by the galaxy's similarity to NGC 5253, we imaged II Zw 40 at 6, 3.6, and 2 cm by using the Very Large Array (VLA) [7] in its A configuration for the maximum angular resolution, and at 11.7 μm with the Long Wavelength Spectrometer (LWS) at the W. M. Keck Observatory.[8] The observations and results are described in the next section and the nature of the source in § 3, in which we also compare the supernebula in II Zw 40 with other dwarf starbursts and discuss the significance of the structure seen in the radio maps.

2. OBSERVATIONS AND RESULTS

2.1. *Radio Images*

II Zw 40 was observed at 6, 3.6, and 2 cm on 1999 August 23, using the VLA in the A configuration. The observations began in late morning with reasonable summer weather. During the run the 12 GHz site monitor rms phase rose from 8° to 20°. Absolute fluxes were calibrated using 3C 286, with fluxes of 3.45, 5.18, and 7.49 Jy at 2, 3.6, and 6 cm, respectively. We estimate absolute flux (scaling) uncertainties of ~5% at 6 and 3.6 cm, and ~7% at 2 cm due to source structure and variability in 3C 286. Missing antennas in the inner array contributed to these uncertainties. For the 2 cm data, we used fast switching with a 50 s calibrator per 100 s source cycle time. We spent 6 minutes, real time, on-source at 6 and 3.6 cm, and 79 minutes, real time, on-source at 2 cm. However, given the fast-switching duty cycle, the actual on-source time at 2 cm was about 44 minutes. The nearby calibrator 0552+032 was used for the fast-switching cycle; we measure a flux of 0.53 Jy for this source. The fast-switching cycles were bracketed with standard calibration scans on the stronger calibrator 0532+075, for which we measure a flux of 1.65 Jy. We applied referenced pointing during the run, with pointing scans taken at 3.6 cm every hour on 0532+075. In this way we were able to obtain reasonable images with the A configuration at 2 cm in daytime summer observing. We estimate, from our mapping of the calibrators, that the seeing at 2 cm with our fast-switching cycle is less than 0.″01, which is the upper limit we fitted to the deconvolved sizes of both calibrators. This is less than a tenth of a beam. Because of the lack of short spacings, the images are insensitive to structures that are more extended than ~30 times the beam. This approximate limit, $\theta_{\rm max}$, is listed for each wavelength in Table 1, along with beam sizes and rms noise levels.

Images at each wavelength are shown in Figure 1. These maps were made with natural weighting. The emission is clearly resolved, especially in the highest-resolution 2 cm map. The position of the 2 cm peak of 0.64 mJy beam^{-1} is $\alpha = 05^{\rm h}55^{\rm m}42^{\rm s}.614 \pm 0^{\rm s}.001$, $\delta = 03^\circ 23' 32''.03 \pm 0''.01$ (J2000.0). The main source is kidney-shaped, hinting that there is further unresolved substructure on size scales less than 0.″4 (20 pc). There is a secondary 2 cm peak, with a flux of 0.54 mJy beam^{-1}, located 0.″23 (11 pc) to the east of the main source, at $\alpha = 05^{\rm h}55^{\rm m}42^{\rm s}.629 \pm 0^{\rm s}.001$, $\delta = 03^\circ 23' 32''.04 \pm 0''.01$. The 6 and 3.6 cm sources are consistent with the structure seen at 2 cm.

Peak fluxes and other information for naturally weighted maps are presented in Table 1. Total mapped fluxes were obtained by integrating the flux radially outward from the peak until it reached a maximum by using Astronomical Image Processing System task IRING. These mapped fluxes are presented in Figure 2 with the single-dish fluxes and other interferometric fluxes from the literature. Most of the 6 and 3.6 cm flux is contained within a radius of 5″–6″. The 2 cm flux is confined to the inner 1.″5 (75 pc) radius region. These size scales are similar to $\theta_{\rm max}$, the angular size at which undersampling effects set in. Of the single-dish emission 60%–80% is concentrated within this central few-arcsecond portion of II Zw 40.

The spectral index of radio continuum emission, which is defined as α in $S_\nu \propto \nu^\alpha$, is −0.1 for pure thermal emission, is some larger negative value, typically −0.6 to −1.2 for nonthermal emission from supernovae events and remnants, and takes on positive values when the radio emission is optically thick. We cannot formally derive the spectral index because the naturally weighted beams at different wavelengths are not matched: the maps at the shorter wavelengths will lose relatively more flux because of undersampling. The spectral index of the overall radio emission in II Zw 40 has been discussed at length in Wynn-Williams & Becklin (1986); Klein et al. (1991); and Deeg et al. (1993). These studies indicate that the centimeter-wave emission of II Zw 40, even at 20 cm, is mostly thermal, and that thermal emission is overwhelmingly dominant at wavelengths less than 6 cm.

[7] The National Radio Astronomy Observatory is a facility of the National Science Foundation operated under cooperative agreement by Associated Universities, Inc.

[8] The W. M. Keck Observatory is operated as a scientific partnership among the California Institute of Technology, the University of California, and the National Aeronautics and Space Administration. The Observatory was made possible by the generous financial support of the W. M. Keck Foundation.

TABLE 1
II Zw 40 Radio Fluxes

λ (cm)	Single-Dish Flux[a] (mJy)	rms (mJy beam^{-1})	Beam (arcsec^2), p.a. (deg)	$\theta_{\rm max}$[b] (FWHM) (arcsec)	Peak Flux (mJy beam^{-1})	Total Mapped Flux[b,c] (mJy)	Fraction of Single-Dish Flux (mJy)	"Matched Beam" Fluxes[d] (mJy)
6.....	22	0.11	0.89 × 0.43, 52	10	3.4	15 ± 1	0.68	9 ± 1.5
3.6.....	21	0.088	0.48 × 0.25, 52	7	1.4	12 ± 1	0.57	10 ± 1.5
2.....	18.5	0.10	0.21 × 0.14, 45	4	0.64	14 ± 1.5	0.75	14 ± 1.5

[a] Extrapolated from values at 4.9, 10.7, and 24.5 GHz; Klein et al. 1991; Klein et al. 1984; Jaffe et al. 1978.

[b] $\theta_{\rm max}$ is the maximum size scale that is well sampled by these images. Fluxes and peak fluxes are therefore lower limits to the total flux.

[c] Total fluxes are obtained by integrating over a circular aperture centered on the peak flux in naturally weighted maps.

[d] "Matched" beam fluxes were obtained by making maps with (u, v) data restricted to baselines greater than 20kλ; these maps are sensitive only to structures smaller than 4″. See text.

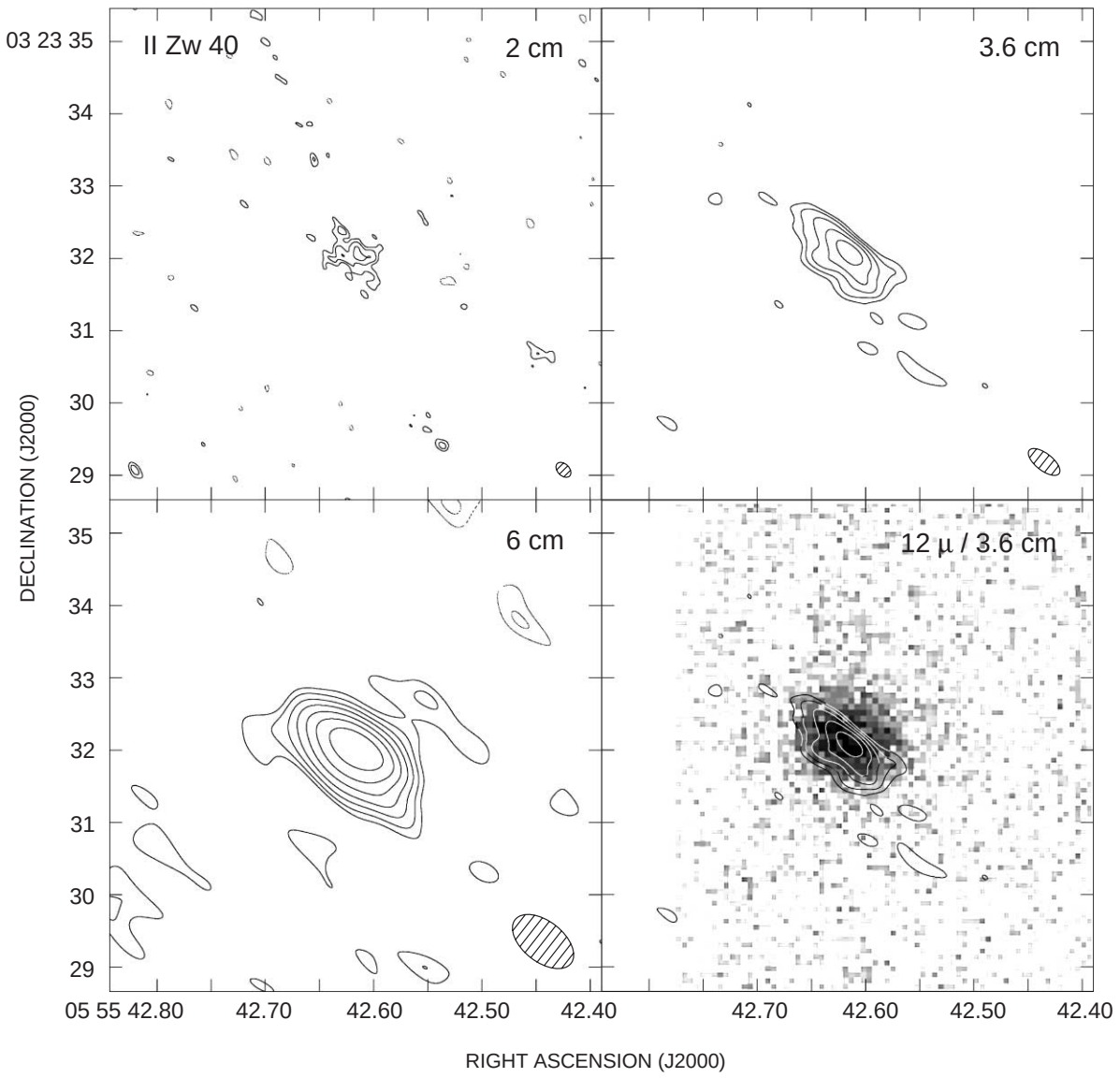

FIG. 1.—Radio and infrared images of II Zw 40. Contours are $\pm 2^{n/2}$ times 0.27 mJy beam^{-1} ($\sim 3\ \sigma$), starting at $n = 0$. Beams are plotted at lower right in each panel. *Top left*: 2 cm VLA map of II Zw 40. Beam is $0''.21 \times 0''.14$, p.a. 45°. *Top right*: 3.6 cm map. Beam is $0''.48 \times 0''.25$, p.a. 52°. *Bottom left*: 6 cm map of II Zw 40. Beam is $0''.89 \times 0''.43$, p.a. 52°. *Bottom right*: 6 cm contours atop the 11.7 μm LWS image of II Zw 40. The seeing in the IR image is estimated to be $0''.2$ to $0''.5$.

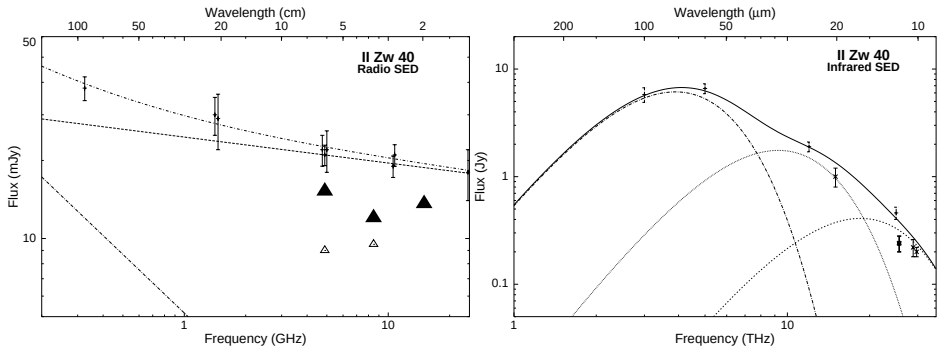

FIG. 2.—Radio and infrared spectral energy distributions for II Zw 40. *Left*: Radio SED of II Zw 40, showing single-dish measurements of Jaffe, Perola, & Tarenghi (1978); Klein, Wielebinski, & Thuan (1984); Klein, Weiland, & Brinks (1991); and Deeg et al. (1993) (*crosses with error bars*), total fluxes from our naturally weighted images (*filled triangles*), fluxes from the images with (u, v) range restricted to match the 2 cm (u, v) coverage (*open triangles*; see text). Statistical uncertainties are ± 1 mJy beam^{-1}; systematic uncertainties due to sidelobes are estimated to be 50% larger. The single-dish data are fitted with an optically thin bremsstrahlung spectrum, $S \propto \nu^{\alpha}$, $\alpha = -0.1$, with a contribution of 21 mJy at 6 cm. The nonthermal synchrotron component is fitted with $\alpha = -0.75$ and a contribution of 12 mJy at 92 cm. *Right*: IR SED of II Zw 40. Fluxes and references are in Table 2.

2.2. 12 μm *Image*

II Zw 40 was observed on the night of 2000 February 17 by using the LWS (Jones & Puetter 1993) on the Keck 1 telescope in imaging mode. The resulting image is shown in Figure 1*d* (*gray scale*) and in Figure 3. The exposure was 486 s through a filter 1 μm wide centered at 11.7 μm. β Gemini and α Bootes were used for calibration. The night was humid and nonphotometric; scatter in the standards was 7% in an hour but as high as 18% over the night, so we conservatively assign 15% uncertainty to the infrared flux. The pixel size is 0.″08 and the chip 128 × 128; the actual resolution, based on the standard star images, is 0.″3 to 0.″5. The infrared source observed is either not or only slightly resolved; the FWHM is ~0.″5. At this resolution the source cannot be distinguished from one that is circularly symmetric.

The total flux at 11.7 μm is 0.24 Jy. This agrees with the 0.22 Jy (Rieke & Low 1972) observed with a 6″ aperture and is more than half the 0.46 Jy seen by IRAS with a beam that took in the entire galaxy. The bright mid-infrared emission indicates that the compact radio source is not a supernova remnant. *The II Zw 40 source has all the radio and infrared behavior of an* H II *region ionized by young OB stars.* The ratio of mid-infrared to thermal 2 cm radio emission is ~20 for this compact radio-IR source, on the low side of the range expected for an H II region (Ho et al. 1990) but quite out of the range of supernovae. The value 12 μm/6 cm is only a factor of 2 greater than the value expected on the basis of Lyα heating alone (Genzel et al. 1982), and it is nearly an order of magnitude smaller than it is in the otherwise very similar supernebula in NGC 5253 (Gorjian et al. 2001). The presence of an infrared excess (IRE) over the value expected from Lyα heating is generally attributed to factors such as the competition of dust and gas for UV photons and the absorption of longer wavelength light by dust. The conditions in II Zw 40—low metallicity and a dominant OB population—may not be conducive to the "normal" IRE.

We list measured IR fluxes from the literature for II Zw 40 in Table 2, including large-aperture IRAS fluxes, and we plot the IR spectral energy distribution (SED) in Figure 2. We fit the SED of II Zw 40 with three dust components, adopting dust emissivities proportional to ν^{β}, where $\beta = 1.5$. The fits are also illustrated in Figure 2.

Our 11.7 μm flux of 0.24 Jy agrees well with the fluxes measured by other groups (Rieke & Low 1972; Wynn-Williams & Becklin 1986) in few-arcsecond apertures and suggests that the mid-IR flux of the central starburst region is confined to the 0.″5 (25 pc) source in our image. The spectrum of this source is rather flat in the mid-IR. It therefore requires fairly warm emission; we can fit it with a dust component of temperature $T \sim 200$ K, giving a luminosity of $L \sim 2.4 \times 10^8\ L_{\odot}$ for this component (see Fig. 2). Dust emission from the supernebula in NGC 5253 and from the dwarf galaxy SBS 0335-052 also indicates hot (200 K) dust, based on high-resolution imaging at 11.7 and 18.7 μm (Gorjian et al. 2001; Dale et al. 2001).

We can estimate a total $L_{\rm IR}$ for II Zw 40 by including IRAS fluxes. The 25 μm IRAS flux of II Zw 40 is due to hot dust with a temperature of ~100 K, we estimate, to explain both the 25 and 60 μm components—again, like NGC 5253. This component (Fig. 2) contributes about $7.2 \times 10^8\ L_{\odot}$,

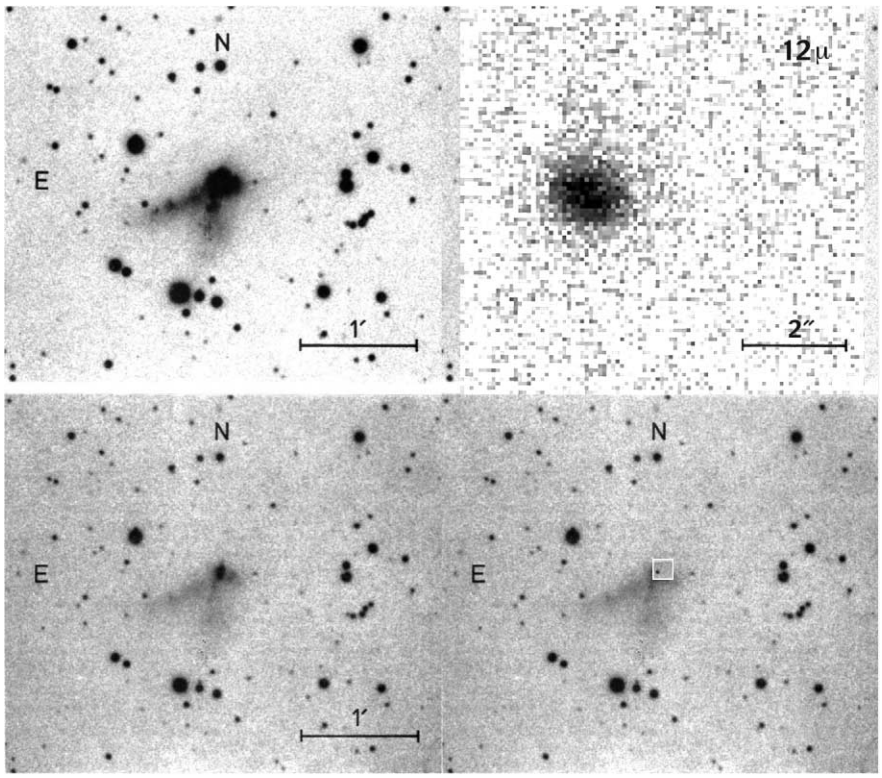

FIG. 3.—*Top left*: Optical image of II Zw 40 from Baldwin, Spinrad, & Terlevich (1982). *Top right*: LWS image of II Zw 40 at 11.7 μm. The entire frame is about 10″ across. *Bottom left*: Blue optical image of II Zw 40 (Baldwin et al. 1982). *Bottom right*: LWS image placed atop the blue optical image to the same scale. The LWS inset is ~10 arcsec^2.

TABLE 2
INFRARED CONTINUUM SPECTRUM

λ (μm)	Flux (Jy)
10.1[a]	0.20 ± 0.02
10.4[b]	0.22 ± 0.04
11.7[c]	0.24 ± 0.04
12[d]	0.46 ± 0.05
20[e]	1.0 ± 0.2
25[d]	1.91 ± 0.2
60[d]	6.61 ± 0.7
100[d]	5.8 ± 0.9

[a] Wynn-Williams & Becklin 1986.
[b] Rieke & Low 1972.
[c] This paper.
[d] Vader et al. 1993; 100 μm flux is affected by Galactic cirrus emission.
[e] Roche et al. 1991.

about 3 times what the 200 K dust contributes. The dust emission is unusually warm in this galaxy (Vader et al. 1993), although the cool (42 K) dust does contribute about half ($9.4 \times 10^8\ L_\odot$) of the total IR luminosity. The 100 μm is also complicated by the presence of Galactic cirrus. From the dust emission out to a wavelength of 100 μm we obtain a total infrared luminosity of $L \sim 1.9 \times 10^9\ L_\odot$.

2.3. *Radio Analysis of the Source: Thermal and Nonthermal Emission and Size Scales*

There is a wealth of radio continuum observations of II Zw 40, both single dish and interferometric, and thus much information on the distribution of thermal and nonthermal emission in the source (Jaffe et al. 1978; Klein et al. 1984; Sramek & Weedman 1986; Klein et al. 1991; Deeg et al. 1993). Vanzi et al. (1996) and Joy & Lester (1988) also discuss the radio structure and the thermal-to-nonthermal flux ratio. Since our A-configuration images do not detect large spatial structures, it is useful to compare them with lower resolution maps and single-dish fluxes, which are sensitive to extended emission.

At 6 cm, the lower resolution VLA images of Wynn-Williams & Becklin (1986) and Sramek & Weedman (1986) revealed 16 mJy of flux within a 20″ region (corresponding to their undersampling radius). The total 6 cm single-dish flux is about 21–22 mJy (Jaffe et al. 1978; Klein et al. 1991). We detect 15 ± 1 mJy at 6 cm, 68% of the total single-dish flux. Vanzi et al. (1996) predict, based on their extinction-corrected Hα flux, a 6 cm flux of 15.7 mJy for a 15″ aperture. Joy & Lester (1988) also conclude that their near-IR and Brγ fluxes are in excellent agreement with the VLA fluxes. From this we conclude that at least 70% of the single-dish 6 cm emission is thermal and confined to a region less than 6″ (300 pc) in extent. The remaining 30% of the single-dish 6 cm emission forms a diffuse extended (>15″, or 750 pc, based on the lower resolution VLA maps of Wynn-Williams & Becklin 1986) halo of thermal emission about this central bright source.

We detect a similar percentage of the total single-dish emission at 2 cm. Our flux of 14 mJy is ~75% of the estimated single-dish emission of 18–19 mJy at 15 GHz (extrapolated from the 10.55, 10.7, and 24.5 GHz measurements of Jaffe et al. 1978; Klein et al. 1991; and Klein et al. 1984). Our 2 cm flux is consistent with the VLA fluxes of Wynn-Williams & Becklin (1986) and Sramek & Weedman (1986) of 12 mJy from lower resolution observations. The 14 mJy of 2 cm flux is confined to within a 3″ diameter region; of this, 10 mJy is found in the inner, 1.″5 diameter, bright "core" region visible in the contour plot of Figure 1. The remaining 4–5 mJy of single-dish flux that is not detected in any of the VLA maps must either be very diffuse, be extended over size scales greater than 20″ (1 kpc), or consist of a spatially extended collection of low-flux sources.

The total 2 cm flux is much greater than the sum of the two peaks seen in the naturally weighted maps. For our flux of 10 mJy for the inner 1.″5 (75 pc) core region, the required Lyman continuum fluxes are at least $No_{\rm Lyc} = 1.0 \times 10^{53}$ s^{-1}, higher if the emission has significant optical depth that it is partly thick at 2 cm. The total mapped 2 cm flux of 14 mJy, which is contained within the inner 3″, requires $N_{\rm Lyc} = 1.4 \times 10^{53}$ s^{-1}.

2.4. "*Matched-Beam*" *Radio Images*

We cannot directly compare fluxes at different wavelengths for the naturally weighted maps of the previous section. This is because the missing short baselines scale to different angular resolutions at the different wavelengths: the spatial scale at which emission is resolved out in the 2 cm maps ($\theta_{\rm max} \sim 3''$–$4''$) is 3 times smaller than for the 6 cm map ($\theta_{\rm max} \sim 10''$). So the maps at each wavelength are missing a different fraction of the true total flux.

It is possible, however, to make maps at different wavelengths for which fluxes can be directly compared. For this we must restrict the baselines in the inner (u, v) plane in the 6 and 3.6 cm maps to match the 2 cm (u, v) restriction. With the current data set, we eliminated all baselines for which $B/\lambda < 20{,}000$. The resulting 6 and 3.6 cm images are noisier than before, but their sensitivity to extended structure is close to that of the 2 cm image. We then convolved these "nearly identical" beams to the Gaussian beam size of the 6 cm map, 0.″88 × 0.″43, p.a. 52°, and compared them.

Total mapped fluxes for these (u, v)-restricted maps, which resemble the naturally weighted 6 cm map, are presented in the last column of Table 1. At 6 and 3.6 cm the "matched beam" images contain less flux than do the naturally weighted images: as the undersampling size scale, $\theta_{\rm max}$, decreases, more of the flux is resolved out. Of the 15 mJy of flux in the naturally weighted 6 cm map ($\theta_{\rm max} \sim 10''$), only 9 ± 1.5 mJy remains in the "matched beam" image; of the 12 mJy of flux in the naturally weighted 3.6 cm image, only 10 ± 1.5 mJy is left in the "matched beam" map. But since the 2 cm map is already restricted with respect to short spacings, the "matched beam" flux is the same as for the naturally weighted map; the 2 cm flux is 14 mJy.

Comparison of the "matched beam" fluxes indicates that the spectral index of the compact ($\theta < 4''$) emission in II Zw 40 is rising from 6 to 2 cm, with a value between +0.4 and +2. This strongly suggests that a significant fraction of the 2 cm free-free emission is not only compact but optically thick.

2.5. *Highest-Resolution Image: The Most Compact Structure*

To further investigate the compact structure, we have mapped the 2 cm emission with the highest possible resolu-

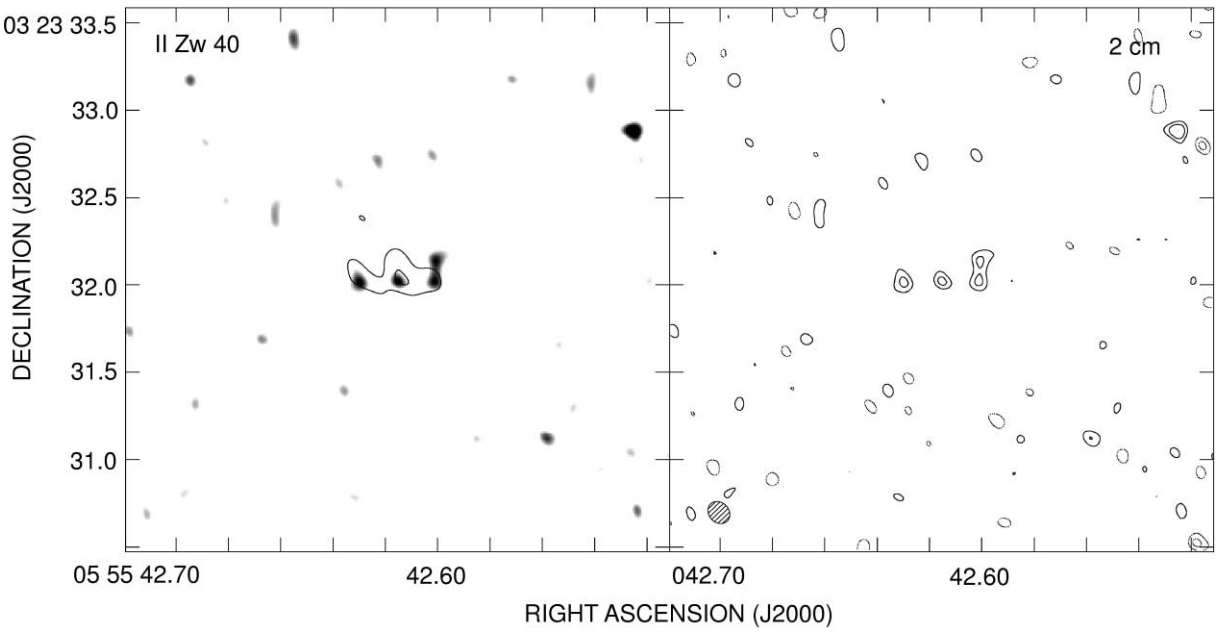

FIG. 4.—*Left*: Uniformly weighted 2 cm VLA map of II Zw 40, in gray scale, with naturally weighted 2 cm map (see Fig. 1) overlaid in contours. The gray-scale range is 0.4–0.6 mJy, ~2.5–4 σ. The uniformly weighted beam is $0\farcs14 \times 0\farcs12$, p.a. 45°. Contours are $2^{n/2}$ times ± 0.4 mJy beam^{-1} (~6 σ for the naturally weighted map), starting at $n = 0$. *Right*: Uniformly weighted 2 cm map. Same contours as for (*a*), ~2.5 σ for this map.

tion, and the result is presented in Figure 4. This map was made with uniform weighting, which places greater weight on the longer baselines. For standard VLA configurations, this sharpens the beam by roughly 50%. The noise in this image, 0.17 mJy beam^{-1}, is a factor of 2 higher than in the naturally weighted map, which is why less emission is seen. The uniform beam is $0\farcs14 \times 0\farcs12$, p.a. 44°.

The uniform image reveals three or four peaks within the central emission region, all of which are 0.59–0.60 mJy beam^{-1}, 3.5 σ. The three strongest peaks are separated by $0\fs015$, or 11 pc. They are at $\alpha = 5^{h}55^{m}42\fs630$, $42\fs615$, and $42\fs601 \pm 0\fs001$, $\delta = 03°23'32\farcs01$, $32\farcs02$, and $32\farcs02 \pm 0\farcs01$ (J2000.0) from east to west, respectively. The first two sources listed also appear as the secondary and main peak in the lower resolution 2 cm image of Figure 1. The fourth source is 6 pc to the north of the westernmost source of the triplet, also 0.6 mJy beam^{-1}, at $\alpha = 5^{h}55^{m}42\fs601 \pm 0\fs001$, $\delta = 03°23'32\farcs13 \pm 0\farcs01$.

These sources may simply be the peaks of the more extended distribution, although there is an increase in brightness temperature with decreasing beam. The 2 cm naturally weighted map has $T_b \sim 120$ K, while the uniform map, with a beam a factor of 1.7 smaller in area, has $T_b \sim 200$ K. This suggests that there is indeed some unresolved structure. The brightest peak in the uniform map, at $\alpha = 5^{h}55^{m}42\fs525$, $\delta = 03°23'32\farcs88$, has a peak flux of 0.76 mJy beam^{-1}, ~5 σ. This peak is located about $1\farcs5$ to the northwest of the center of the triplet. There is little extended emission associated with this source, as it is not strong in the lower resolution images.

We can estimate the source sizes by using the spectrum and the intensities observed here. Peak flux densities of ~0.6 mJy beam^{-1} for the quadruplet correspond to brightness temperatures of ~200 K for the $0\farcs14$ by $0\farcs12$ beam. For this brightness to be consistent with the rising spectrum and optically thick emission, the source must be confined to a region smaller than the beam size. For an electron temperature of 13,000 K, as determined from optical lines by Walsh & Roy (1993), and for $\tau \sim 1$, we estimate that a source diameter of $d \sim 1$ pc would produce the observed brightness. The emission measure implied by a turnover frequency of 15 GHz is about 10^9 cm^{-6} pc, and the corresponding nebular density would then be $\sim(3\text{–}4) \times 10^4$ cm^{-3}. Emission measures and densities of these magnitudes are seen only in the youngest H II regions in the Galaxy. This suggests that these nebulae are very young. The dynamical time for the expansion of an H II region to this size at a sound speed of 10 km s^{-1} is ~10^5 yrs; its size is another suggestion of its likely youth.

For each source within the quadruplet, we find a lower limit to the Lyman continuum of $N_{\rm Lyc} \sim 6 \times 10^{51}$ s^{-1} for $\tau = 0$ (optically thin), $N_{\rm Lyc} = (0.8\text{–}1) \times 10^{52}$ s^{-1} for $\tau = 1$, and higher if $\tau > 1$.

2.6. *Comparison with Brγ; Extinction in the Nebula*

Brγ fluxes have been obtained and analyzed by several groups, including Wynn-Williams & Becklin (1986) and Joy & Lester (1988). Vanzi et al. (1996) and Davies et al. (1998) have actually imaged Brγ. We can compare our high-resolution free-free fluxes with their results to estimate extinctions.

We measure 14 mJy of free-free emission at 2 cm in II Zw 40, from a region ~3″ in diameter. Using the recombination emissivities of Hummer & Storey (1987) for 12,500 K, we would predict on the basis of the 2 cm free-free flux a Brγ flux of $S^{\rm pred}_{\rm Br\gamma} = 1.2 \times 10^{-13}$ ergs s^{-1} cm^{-2}. This can be compared with the $S^{\rm obs}_{\rm Br\gamma} = (0.3\text{–}0.4) \times 10^{-13}$ ergs s^{-1} cm^{-2} measured by Vanzi et al. (1996) in an aperture of 3″–4″, and $S^{\rm obs}_{\rm Br\gamma} = 0.4 \times 10^{-13}$ ergs s^{-1} cm^{-2} measured by Davies et al. (1998). The extinction at 2.2 μm implied by the difference is $A_K \sim 1\text{–}1.2$, for a visual extinction of $A_V \sim 8\text{–}10$ mag

(adopting the extinction curve of Rieke & Lebofsky 1985). Based on comparisons of Hα and Brγ fluxes, Joy & Lester (1988), Vanzi et al. (1996), and Davies et al. 1998) estimate $A_K \sim 0.32$–0.36, a factor of 3 lower than we find. It is likely that the apparent contradiction is caused by the fact that much of the extinction is high and internal to the nebula. Infrared line ratios frequently give higher extinctions than do visible line ratios (Beck, Turner, & Ho 1986). $A_K \sim 1$ mag is seen in many starbursts of this luminosity (Ho et al. 1990; Kawara et al. 1989).

We interpolate a single-dish flux of 18.5 mJy at 2 cm from the 2.88 and 1.18 cm measurements of Klein et al. (1991) and Klein et al. (1984). For apertures larger than $\sim 4''$ we would predict a Brγ flux of $S^{\rm pred}_{\rm Br\gamma} = 1.6 \times 10^{-13}$ ergs s^{-1} cm^{-2}, which can be compared with the observed flux of $S^{\rm obs}_{\rm Br\gamma} = 7 \times 10^{-14}$ ergs s^{-1} cm^{-2} measured by Vanzi et al. (1996) for a $15''$ aperture and Moorwood & Oliva (1988) in a $6'' \times 6''$ aperture. From these fluxes we estimate $A_K \sim 0.96$, or $A_V \sim 8$ for emission on larger ($r > 200$ pc) size scales.

3. NATURE AND STELLAR POPULATION OF THE SOURCE

The infrared and radio emission from II Zw 40 has the form of a concentrated $1\farcs5$ (75 pc) diameter core containing at least half (10 mJy) of the large aperture flux, within a slightly larger ($3''$, 150 pc diameter, 14 mJy) region of lower level (2–2.5 σ) extended emission, and diffuse thermal emission extended on larger scales, which cannot be detected in these images. Our further discussion will concentrate on the compact thermal sources detected in these maps.

The number of stars needed to ionize the radio source can be estimated from the total ionization of 1.4×10^{53} s^{-1}. This requires $\sim 1.4 \times 10^4$ typical O7 stars over the central $3''$ (150 pc) region, of which 10^4 are confined to the inner 75 pc core. If the stars follow the nebular emission—as seems to be the case in NGC 5253—then from its appearance in the highest-resolution map II Zw 40 is currently forming at least four parsec-sized clusters with $\sim$600 O stars each. For a Salpeter zero-age main-sequence (ZAMS) initial mass function (IMF) down to 1 $M_\odot$, these four clusters would have masses of $\sim 10^5$ $M_\odot$, higher if the IMF extends to below 1 $M_\odot$. The estimated mass for the entire 150 pc region would be at least $\sim 2 \times 10^6$ $M_\odot$ (O3 to G).

The luminosity of this large population of young stars is consistent with the IR spectrum, in which the mid-infrared contribution is substantial. The total observed IR luminosity out to 100 μm is $L_{\rm IR} \sim 1.9 \times 10^9$ $L_\odot$. We estimate, using a Salpeter ZAMS IMF with upper mass cutoff of O3 (following Turner et al. 1998) that the ratio of ZAMS luminosity to Lyman continuum photons is $N_{\rm Lyc} \sim 2 \times 10^{-44}$ s^{-1}. Then our Lyman continuum rate of 1.4×10^{53} s^{-1} implies an OB luminosity of $L_{\rm OB} \sim 3 \times 10^9$ $L_\odot$. This OB luminosity is very similar to $L_{\rm OB}$ obtained by Vanzi et al. (1996) on the basis of emission-line excitation. $L_{\rm OB}$ may exceed $L_{\rm IR}$, although there are uncertainties in the SED and in the fit and in $L_{\rm OB}$. What is clear, however, is that the current starburst is responsible for the infrared luminosity; even a ZAMS OB luminosity appears to overpredict $L_{\rm IR}$. This suggests that the starburst is exceedingly young or that there are unusually massive stars, O2 or above, as might be suggested by comparison with the smaller and less extreme cluster R136 (Massey & Hunter 1998). The thermal radio and infrared source, which we call the supernebula because of its similarity in all but size to a normal H II region, provides all the infrared luminosity in II Zw 40. In fact, in this galaxy, the infrared luminosity may fall short of measuring the true star formation rate.

We would like to emphasize a point made by Vanzi et al. (1996): the radio-to-IR correlation seen in many galaxies does not hold in II Zw 40, since the centimeter-wave fluxes fall short of the value predicted by the radio-IR correlation by factors of 6–10. Given that the IR excess in this galaxy appears to be low, based on the thermal radio fluxes, this discrepancy is even more notable. There is just not much nonthermal synchrotron emission in this blue compact dwarf for the magnitude of its star formation. This is consistent with the starburst being extremely young. However, the very similar starburst in NGC 5253 shows a similar lack of nonthermal emission even though it has clusters estimated to range from 2.5–50 Myr (Calzetti et al. 1997; Tremonti et al. 2001). It is unclear whether the lack of nonthermal synchrotron emission from these starbursting dwarfs is due to the youth of the starburst or to some other cause, such as the lack of a global magnetic field (Turner et al. 1998).

3.1. *Structure of the Starburst in II Zw 40: Multiple Star Clusters?*

The starburst in II Zw 40 clearly has a complex radio structure, best seen in our 2 cm map (Figs. 1*a* and 3). In the highest-resolution uniform maps there are at least four sources visible within a region of emission that extends to a diameter of 150 pc. Under the very rough assumptions of the earlier sections we estimate that the starburst contains 14,000 O7 star equivalents. The starburst appears to be made up of four compact 1 pc diameter nebulae excited by clusters each containing $\sim$600 O stars and $\sim 10^5$ $M_\odot$. The individual nebulae or clusters are separated by 10–12 pc. These characteristics are similar to the supernebulae in NGC 5253, He 2-10, and NGC 2146 (Beck et al. 1996; Turner et al. 1998; Kobulnicky & Johnson 1999; Turner et al. 2000; Tarchi et al. 2000; Beck et al. 2001). But it should be noted that what we refer to as "clusters" and "sources" are not isolated and well-defined emission regions, like globular clusters in our Galaxy. Rather, these are emission peaks within an extended region of emission. In this sense the nebulae resemble large Galactic H II region complexes such as W49 and W51. It would be very worthwhile to reobserve this galaxy with the highest possible resolution and better signal-to-noise ratio.

If the O stars deduced from the radio flux formed alongside the usual number of smaller stars, there will be a total mass of $\sim 2 \times 10^6$ $M_\odot$ in young stars within the 150 pc volume of the starburst, and an estimated 10^6–10^7 young stars. This stellar density is high but not extraordinary; NGC 5253, for example, has an estimated 1 million stars within a region 1 by 2 pc (Turner et al. 2000). However II Zw 40 is a tiny galaxy. Sargent & Searle (1970), Joy & Lester (1988), and Vanzi et al. (1996) all point out that the OB mass of II Zw 40 is a remarkably high (10%) fraction of its total stellar mass, which Vanzi et al. (1996) estimate at $M \sim 2 \times 10^7$ $M_\odot$.

The 75 pc extent of the starburst core places constraints on the trigger for the starburst. The crossing time for a disturbance moving at the sound speed in 10^4 K gas is roughly 5–10 Myr. While it is difficult to place ages on these nebulae,

comparison with Galactic H II regions of similar properties would give the nebulae ages of less than 1 Myr (Gorjian et al. 2001). The ages of these sources are almost certainly a small fraction of the crossing time of the region, suggesting that the star formation was triggered nearly simultaneously. It seems unlikely, therefore, that "sequential super–star cluster formation" is operating in II Zw 40.

How does the structure seen in II Zw 40 compare with that in other supernebula-dominated systems? II Zw 40 is like NGC 5253 and He 2-10 in that the infrared and radio fluxes come from obscured super–star clusters. The II Zw 40 source is more luminous than the NGC 5253 supernebula in the radio and infrared and contains at least twice the number of O stars, but they are distributed in multiple sources over a much larger volume. The total stellar content of the II Zw 40 source is close to that of the main source A in the dwarf galaxy He 2-10 (Kobulnicky & Johnson 1999; Beck et al. 2001; Vacca et al. 2002), which it also resembles in size and radio and infrared flux. He 2-10 has not been observed with high resolution so the possibility of discrete subclusters within the main sources is open. Why is the starburst in II Zw 40 concentrated within 75 pc, that in He 2-10 within 200 pc, that in SBS 0335-052 within 1000 pc (Dale et al. 2001; Izotov et al. 1997), and that in NGC 5253 within only 2 pc? That must depend on the interactions that triggered the formation of the massive star clusters in the first place and their subsequent evolution.

4. CONCLUSIONS

Our high-resolution radio and infrared observations of the starburst dwarf galaxy II Zw 40 have found that the radio emission at 6, 3.6, and 2 cm is thermal free-free emission with ~70%–75%, of the centimeter-wave emission confined to a region less than 3″ in diameter. Within this region there is a bright core of diameter ~1.″5 (75 pc) containing at least four subsources. The spectrum of the compact emission appears to be rising between 3.6 and 2 cm, suggesting that the free-free emission is optically thick at 2 cm, with implied emission measure of EM $\sim 10^9$ cm^{-6} pc and electron density $n_e \sim (3\text{–}4)\times 10^4$ cm^{-3}. For optically thick emission, the observed brightnesses require that the emitting sources be ~1 pc diameter H II regions, with $N_{\rm Lyc} \sim 6 \times 10^{51}$ s^{-1}. The 75 pc "core" starburst region is a complex of four compact "supernebulae," each powered by ~600 O stars, with an estimated $\sim 10^5\ M_\odot$ in young stars in each cluster. The supernebulae or clusters are separated by ~12 pc. The total ionization of II Zw 40 is at least $N_{\rm Lyc} = 1.4 \times 10^{53}$ s^{-1}, or 14,000 O7 star equivalents. For a Salpeter ZAMS IMF, we estimate that roughly 1–10 million young stars and a young stellar mass of $2 \times 10^6\ M_\odot$ are present within II Zw 40. The total young stellar luminosity is $L_{\rm OB} \sim 3 \times 10^9\ L_\odot$. The OB luminosity is in good agreement with or perhaps even higher than the observed infrared luminosity of $L_{\rm IR} \sim 1.9 \times 10^9\ L_\odot$. The radio-infrared ratios in this galaxy differ from the usual starburst values; we attribute this to the extreme youth of the star formation activity, the low metal content of the gas, and a very weak cool dust component.

We are grateful to S. Van Dyk for assistance with the 6 cm data and to an anonymous reviewer for helpful comments. This work was supported in part by NSF grant AST 00-71276 to J. L. T. and by the Israel Academy Center for Multi-Wavelength Astronomy grant to S. C. B. This research has made use of the NASA/IPAC Extragalactic Database, which is operated by the Jet Propulsion Laboratory, California Institute of Technology, under contract with the National Aeronautics and Space Administration. The authors wish to recognize the significant cultural role that the summit of Mauna Kea has had within the indigenous Hawaiian community and are grateful for the opportunity to conduct observations from this mountain.

REFERENCES

Baldwin, J. A., Spinrad, H., & Terlevich, R. 1982, MNRAS, 198, 535
Beck, S. C., Crowther, P., & Conti, P. 2002, in preparation
Beck, S. C., Turner, J. L., & Gorjian, V. 2001, AJ, 122, 1365
Beck, S. C., Turner, J. L., & Ho, P. T. P. 1986, ApJ, 309, 70
Beck, S. C., Turner, J. L., Ho, P. T. P., Lacy, J. H., & Kelly, D. 1996, ApJ, 457, 610
Brinks, E., & Klein, U. 1988, MNRAS, 231, P63
Calzetti, D., Meurer, G. R., Bohlin, R. C., Garnett, D. R., Kinney, A. L., Leitherer, C., & Storchi-Bergmann, T. 1997, AJ, 114, 1834
Crowther, P. A., Beck, S. C., Willis, A. J., Conti, P. S., Morris, P. W., & Sutherland, R. S. 1999, MNRAS, 304, 654
Dale, D. A., Helou, G., Neugebauer, G., Soifer, B. T., Frayer, D. T., & Condon, J. J. 2001, AJ, 122, 1736
Davies, R. I., Sugai, H., & Ward, M. J. 1998, MNRAS, 295, 43
Deeg, H.-J., Brinks, E., Duric, N., Klein, U., & Skillman, E. 1993, ApJ, 410, 626
Genzel, R., Becklin, E. E., Wynn-Williams, C. G., Moran, J. M., Reid, M. J., Jaffe, D. T., & Downes, D. 1982, ApJ, 255, 527
Gorjian, V., Turner, J. L., & Beck, S. C. 2001, ApJ, 554, L29
Ho, P. T. P., Beck, S. C., & Turner, J. L. 1990, ApJ, 349, 57
Hummer, D. G., & Storey, P. J. 1987, MNRAS, 224, 801
Izotov, Y. I., Lipovetsky, V. A., Chaffee, F. H., Foltz, C. B., Guseva, N. G., & Knaiazev, A. Y. 1997, ApJ, 476, 698
Jaffe, W. J., Perola, G. C., & Tarenghi, M. 1978, ApJ, 224, 808
Jones, B., & Puetter, R. 1993, Proc. SPIE, 1946, 610
Joy, M., & Lester, D. F. 1988, ApJ, 331, 145
Kawara, K., Nishida, M., & Phillips, M. M. 1989, ApJ, 337, 230
Klein, U., Weiland, H., & Brinks, E. 1991, A&A, 246, 323
Klein, U., Wielebinski, R., & Thuan, T. X. 1984, A&A, 141, 241
Kobulnicky, H. A., & Johnson, K. E. 1999, ApJ, 527, 154
Massey, P., & Hunter, D. A. 1998, ApJ, 493, 180
Meier, D. S., Turner, J. L., & Beck, S. C. 2002, AJ, 124, 877
Moorwood, A. F. M., & Oliva, E. 1988, A&A, 203, 278
Rieke, G. H., & Lebofsky, M. J. 1985, ApJ, 288, 618
Rieke, G. H., & Low, F. J. 1972, ApJ, 176, L95
Roche, P. R., Aitken, D. K., Smith, C. H., & Ward, M. J. 1991, MNRAS, 248, 606
Sage, L. J., Salzer, J. J., Loose, H.-H., & Henkel, C. 1992, A&A, 265, 19
Sargent, W. L. W. 1970, ApJ, 160, 405
Sargent, W. L. W., & Searle, L. 1970, ApJ, 162, L155
Sramek, R. A., & Weedman, D. W. 1986, ApJ, 302, 640
Tarchi, A., Neininger, N., Klein, U., Greve, A., Garrington, S. T., Muxlow, T. W. B., Pedlar, A., & Glendenning, B. E. 2000, A&A, 358, 95
Thornley, M., Schreiber, N. M. F., Lutz, D., Genzel, R., Spoon, H. W. W., Kunze, D., & Sternberg, A. 2000, ApJ, 539, 641
Tremonti, C. A., Calzetti, D., Leitherer, C., & Heckman, T. M. 2001, ApJ, 555, 322
Turner, J. L., Beck, S. C., & Ho, P. T. P. 2000, ApJ, 532, L109
Turner, J. L., Ho, P. T. P., & Beck, S. C. 1998, AJ, 116, 1212
Vacca, W. D., & Conti, P. S. 1992, ApJ, 401, 543
Vacca, W. D., Johnson, K. E., & Conti, P. S. 2002, AJ, 123, 772
Vader, J. P., Frogel, J. A., Terndrup, D. M., & Heisler, C. A. 1993, AJ, 106, 1743
van Zee, L., Skillman, E. D., & Salzer, J. 1998, AJ, 116, 1186
Vanzi, L., Rieke, G. H., Martin, C. L., & Shields, J. C. 1996, ApJ, 466, 150
Walsh, J. R., & Roy, J.-R. 1993, MNRAS, 262, 27
Wynn-Williams, C. G., & Becklin, E. E. 1986, ApJ, 308, 620